Ion and velocity map imaging for surface dynamics and kinetics

Dan J. Harding, Jannis Neugebohren, Hinrich Hahn, D. J. Auerbach, T. N. Kitsopoulos, and Alec M. Wodtke

Citation: The Journal of Chemical Physics **147**, 013939 (2017); doi: 10.1063/1.4983307
View online: http://dx.doi.org/10.1063/1.4983307
View Table of Contents: http://aip.scitation.org/toc/jcp/147/1
Published by the American Institute of Physics

Ion and velocity map imaging for surface dynamics and kinetics

Dan J. Harding,[1,2,a)] Jannis Neugebohren,[1,2] Hinrich Hahn,[1,2] D. J. Auerbach,[1,2] T. N. Kitsopoulos,[1,2,3,4] and Alec M. Wodtke[1,2,5]
[1]*Institut für Physikalische Chemie, Georg-August-Universität Göttingen, Tammannstraße 6, 37077 Göttingen, Germany*
[2]*Max-Planck-Institut für biophysikalische Chemie, Am Faßberg 11, 37077 Göttingen, Germany*
[3]*Department of Chemistry, University of Crete, 71003 Heraklion, Greece*
[4]*Institute of Electronic Structure and Laser, Foundation for Research and Technology-Hellas, 71003 Heraklion, Greece*
[5]*International Center for Advanced Studies of Energy Conversion, Georg-August-Universität Göttingen, Tammannstraße 6, 37077 Göttingen, Germany*

(Received 28 February 2017; accepted 28 April 2017; published online 17 May 2017)

We describe a new instrument that uses ion imaging to study molecular beam-surface scattering and surface desorption kinetics, allowing independent determination of both residence times on the surface and scattering velocities of desorbing molecules. This instrument thus provides the capability to derive true kinetic traces, i.e., product flux versus residence time, and allows dramatically accelerated data acquisition compared to previous molecular beam kinetics methods. The experiment exploits non-resonant multiphoton ionization in the near-IR using a powerful 150-fs laser pulse, making detection more general than previous experiments using resonance enhanced multiphoton ionization. We demonstrate the capabilities of the new instrument by examining the desorption kinetics of CO on Pd(111) and Pt(111) and obtain both pre-exponential factors and activation energies of desorption. We also show that the new approach is compatible with velocity map imaging. *Published by AIP Publishing.* [http://dx.doi.org/10.1063/1.4983307]

INTRODUCTION

Dynamical processes occurring during the interaction of atoms and molecules with surfaces are intimately related to the reaction rates which are important to understanding heterogeneous catalysis. Depending upon the nature of the surface and the type, energy, and orientation of the atom or molecule, a wide range of processes may occur at the gas-surface interface, ranging from direct scattering (H/Au(111),[1] NO/Ag(111),[2] N_2/Au(111)[3]) to trapping-desorption (CO/Pt(111)[4]), dissociative adsorption (CH_4/Pt(111),[5] H_2O/Ni(111), HCl/Au(111)[6]), and associative desorption (H_2/Cu(111)[7]).

Experimentalists have employed molecular beam scattering methods to observe the speed and angular distributions, which serve as dynamical fingerprints, to provide details about the potential energy surface (PES) on which the scattering occurs, and the mechanisms of energy transfer between the molecule and the solid. Examples serve to demonstrate the insights gained in this way. The high translational energy of desorbing H_2 molecules formed by the recombination of H-atoms on Cu(111) revealed the barrier height to dissociation of the gas phase H_2 on the surface, via detailed balance.[7] The large kinetic energy loss of H-atoms directly scattered from a Au(111) surface showed that the excitation of electron-hole pairs in the metal plays an important role in the scattering and adsorption processes.[1] Deviations from Maxwellian velocity distributions and from cos(θ) (with respect to the surface normal) angular distributions for argon atoms desorbing from Pt(111) provided velocity and incidence angle dependent sticking probabilities, again via detailed balance.[8] The surface temperature dependence of the vibrational excitation probabilities of NO,[9] N_2,[3] and CO[10] on Au(111), combined with the absence of a threshold in the incidence energy dependence provided a fingerprint for the electronically non-adiabatic vibrational excitation. From these examples, it is clear that the experimental observation of the dynamical fingerprints of the different processes controlling surface scattering require accurate measurement of the laboratory-frame speed and angular distributions of scattered molecules as a function of the surface temperature (T_s) and the molecules' incidence energy and initial quantum state.

Molecular beam methods combined with electron bombardment ionization (EI) based mass spectrometric detectors have also been employed to observe the *kinetics* of surface reactions.[11–13] Despite their proven track record of usefulness, these methods suffer from two fundamental problems. First, EI based mass spectrometry reports the molecular density, whereas, the kinetics require measurements of flux. Second, in any practical instrument, the EI detector must be placed at a finite distance from the surface; hence, time dependent signals from which kinetics are to be derived are a convolution of the surface residence time distribution, which is fundamental to the kinetics, and the flight time distribution of the molecules traveling from the surface to the ionizer.

These two fundamental problems have recently been solved in an experiment that simultaneously measures dynamical and kinetic properties of molecule surface interactions. Specifically, the accurate kinetics of CO desorption from

a)daniel.harding@mpibpc.mpg.de

Pt(111) were obtained in a two-laser UV-UV double resonance tagging experiment, where the residence time and the desorbing molecules' speed could be measured independently in a molecular beam scattering experiment.[4] Here, the delay between a short pulsed molecular beam and a pulsed UV probe laser detecting desorbing CO molecules very close to the surface was used to measure the residence time directly. The density of the UV pumped CO $a^3\Pi_1$ molecules and their speed was obtained by selective Resonance Enhanced Multiphoton Ionization (REMPI) of CO $a^3\Pi_1$ using a temporally delayed laser pulse several centimeters away from the surface. By varying the distance and the delay between the two laser pulses, different speeds could be probed. While this approach was effective and elegant, it cannot be directly generalized to other molecules due to the specificity of the double resonance spectroscopy used in the experiment.

In this paper, we show how this concept can be generalized and improved with ion imaging.[14] To prove its accuracy, we demonstrate this new approach by measuring the desorption kinetics of CO from Pt(111) and Pd(111), which have been previously studied.[15–29] As in the double resonance experiment, the residence time and the speed are measured independently—ion imaging is used to record the speeds and angles of the desorbing CO molecules and the timing between a short pulsed molecular beam and the ionizing laser reports on the residence time at the surface. To make the method useful for a wider variety of molecules, we use non-resonant multiphoton ionization accomplished with a high power 150-fs laser pulse in the near infrared. Furthermore, we employ an experimental geometry that allows very rapid data acquisition as well as velocity map imaging (VMI).

EXPERIMENTAL DETAILS

Figure 1 shows a schematic of the apparatus. The molecular beam chamber is a single stainless steel vessel subdivided into five regions allowing the formation of two differentially pumped molecular beams. Each source chamber has its own pump (2300 L/s Turbomolecular Pump—TMP) as does each first differential pumping region (DP1, 700 L/s TMP). The second differential pumping region (DP2, 700 L/s TMP) is shared by both beams. The main beam is mounted on the

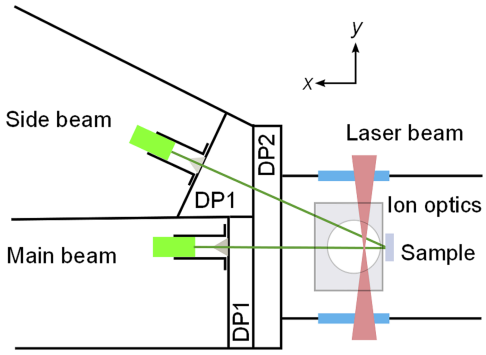

FIG. 1. Schematic of the source and main chambers of the instrument. A differentially pumped molecular beam is used to dose the Pt(111) surface (sample) with CO. Non-resonant multiphoton ionization is effected by a tightly focused laser pulse (red) and ion images are recorded out of the plane of the figure. The first (DP1) and second (DP2) differential pumping regions are labeled. See also Fig. 2.

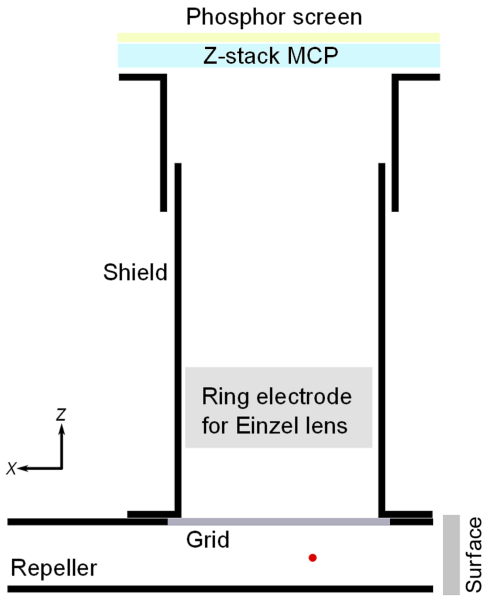

FIG. 2. Schematic of imaging ion optics. The ionization laser position is shown by the red point. Ions formed here are extracted upwards by a pulsed electric field that is switched on a short time (typically 1-2 μs) after the ionization laser. Spatial imaging provides accurate speed information on the desorbing CO molecules. The delay between the pulsed CO beam and the ionizing laser pulse provides information on the CO residence time.

center axis of the machine and the side beam is mounted at an angle of 23°. The surface is held at the crossing point of the two beams during scattering measurements. The size of each beam is controlled using a skimmer and an aperture in the wall dividing DP2 from the main chamber. The pulsed valves are held in "bird cage" mounts that accept home built piezo-valves (used in the work described here), home built solenoid valves, or commercial general valves. The "bird cage" provides the alignment of the beam while allowing the nozzle-skimmer distance to be varied.

The main experimental chamber houses ion optics and a detector for ion imaging, which is performed along an axis out of the plane of Fig. 1 after ionization by non-resonant multiphoton ionization (the laser beam is shown in red). We define the axes in the machine as the x-direction is along the main molecular beam axis, the y-direction is along the laser beam axis, and the z-direction is toward the imaging detector.

The metal surface is mounted to a sample manipulator and can be positioned as shown in Fig. 1 for scattering measurements or retracted to another position where the sample preparation is accomplished with Ar-ion sputtering, annealing, and Auger electron spectroscopy (AES).

Others have previously reported using position sensitive detection methods for studying surface scattering,[30] based on ion imaging[31–33] or velocity map imaging techniques, which were developed at around the same time as those for the gas-phase imaging experiments.[34,35] These have predominantly used a geometry in which the surface and the detector are parallel,[36–41] which is convenient for the production of the imaging electric fields but prevents the projection of the full velocity distribution in the scattering plane onto the detector. Our new imaging setup (shown in Fig. 2) has similarities with an ion scattering experiment of Jacobs,[42] using a similar

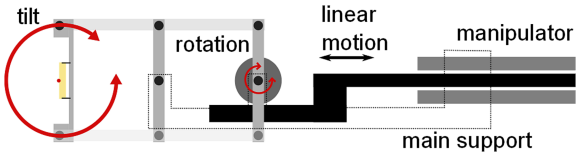

FIG. 3. Schematic drawing of the sample holder. Linear motion of the auxiliary drive is converted to the rotational "tilt" motion and transferred to the sample by the parallelogram linkage. The center of rotation at the sample surface is shown by the red point. The entire assembly is attached to a horizontally mounted manipulator that can be rotated about its axis to vary the azimuthal (ϕ) incidence angle.

geometry, with the surface and detector perpendicular, and pulsed extraction fields. It consists of a repeller electrode, an extractor grid electrode, and a grounded metal tube which together with a ring electrode form an external Einzel lens. In addition to forming part of the Einzel lens, the grounded tube also acts as a shield, preventing stray fields from influencing the ions' flight paths and stray light from reaching the imaging detector. With the proper voltage applied to the ring electrode, velocity map imaging can be performed—when grounded, the system operates in the spatial imaging mode. Ions are detected by a z-stack of three microchannel plates (MCP) and a phosphor screen (ProxiVision P43). The images are recorded using a LaVision E-lite CCD camera and the LaVision on LaVison Davis software.

The repeller and grid electrodes are made with an ultrafine electroformed grid (Precision Eforming, 670 lines/in., 49% transmission), which is stretched and heated prior to being glued to its support frame with graphite paste. The electrodes generate a homogeneous electric field, which projects ions from their initial positions toward the detector whilst preserving their spatial distribution and velocity in the *xy*-plane. The spatial resolution in this mode is limited by the size of the molecular beam. We use a combination of laser slicing,[43] delayed pulsed extraction, and fast gated pulsed MCPs to slice[44] the molecular and ion distributions. This has the benefit of improving the speed and angular resolution in the *xy*-scattering plane and removes the need to perform an Abel inversion to recover the 3-dimensional scattering distribution.

The home built sample holder—shown in Fig. 3—is mounted on a 4-axis (x, y, z, ϕ) horizontal manipulator (VG Scienta) allowing the sample to be moved between sputtering, AES, and measurement regions. To allow proper alignment for sputtering, AES, and measurements, it is necessary for the surface to be tilted by up to 90° and rotated up to 270° in ϕ. In order to achieve this range of motion, while maintaining unrestricted optical and spatial access, we have used a mechanism where the sample rotates around a virtual pivot centered on the front face of the crystal, allowing the tilt angle to be changed without changing the position at which scattering occurs. The linear motion from the manipulator is converted to rotation using a rack-and-pinion. The rotational motion is transferred by the parallelogram linkage to the sample. Offsetting the mounting hardware from the line of centers of the parallelogram bearings allows the face of the crystal to be placed at the center of rotation, which in turn allows the tilt angle to be changed without altering the distance between the surface and the molecular beam source or ion optics. The sample, mounted to the holder with tungsten wires, can be heated via pulsed electron bombardment (to at least 1400 K) or cooled with liquid nitrogen. The sample temperature is measured with a type-K thermocouple and controlled by a Proportional-Integral-Derivative (PID) circuit which modulates the filament current. A negative bias voltage (−500 V) is applied to the filament for EB heating; this is switched to ground shortly before the laser pulse and only switched back on after the ions have been detected, ensuring that the bias voltage does not influence the electric fields within the ion optics.

APPLICATION: CO TRAPPING-DESORPTION FROM Pd(111) AND Pt(111)

In these experiments, the Pd(111) and Pt(111) surfaces were cleaned using cycles of argon ion sputtering and annealing (873 K for Pd(111) and 1303 K for Pt(111)), until no impurities (especially carbon) could be detected by AES following annealing. AFM images of the Pt(111) crystal found the average step density to be 0.05%, significantly flatter than the crystal used by Golibrzuch *et al.* (0.5%).[4]

After dosing the surface with a pulse of CO, ionization of desorbing CO was performed using a Ti:sapphire laser (775 nm, 1 mJ/pulse, 150 fs pulse) which was brought to a focus 20 mm in front of the metal surface with a 200 mm focal length lens. The laser intensity at the focus is sufficient to induce non-resonant multiphoton ionization (fs-MPI). One advantage of fs-MPI is the fact that only the molecules very near to the focus of the laser are ionized. We positioned the focus to probe molecules desorbing near to the surface normal. The surface was dosed with CO using the side beam—see Fig. 1—as this allows us to avoid ionization of molecules in the incident beam. Scanning the focus across the ionization region by moving the focusing lens on a stepper motor driven translation stage allows the angular distribution to be constructed.

The mass/charge ratio of the detected ions is selected using the "gate" timing delay between the HV pulses to the repeller and the MCP, which determines the time-of-flight and hence the mass/charge ratio of the detected ions. When combined with delayed extraction, the short pulse provided by the MCP gate can also be used to slice the ion distribution.[14,44] The desorption kinetics are measured by varying the delay between the molecular beam dosing pulse and the probe laser pulse. At each delay, an ion image of the desorbing CO is recorded.

Figure 4(a) shows a composite image of desorbing CO normal to the surface summed over the full range of beam-laser delays. This contains information about the full speed distribution of the CO desorbing normal to the Pd(111) surface. Using this image, we can determine the speed distribution (shown in Fig. 4(b)). We then have some freedom to choose a suitable speed—defined by a region of the pixels in the image—at which to measure the CO desorption kinetics. Specifically, we chose a part of the image corresponding to probing speeds between 800 ms^{-1} and 1000 ms^{-1}. This suppresses the signal from the background CO with a translational temperature of 300 K caused by the reflected molecular beam. More concretely, we chose an integration region of 20 pixels × 50 pixels

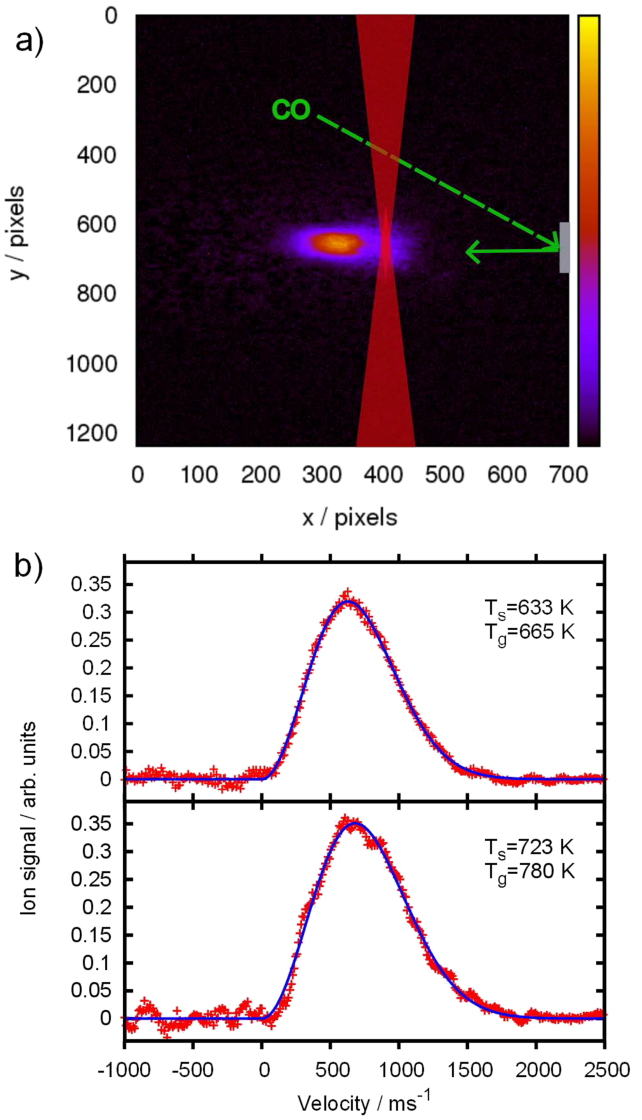

FIG. 4. Speeds of desorbing CO molecules obtained by spatial ion imaging with non-resonant multiphoton ionization. (a) Composite ion image of CO desorbing from a Pd(111) surface and the positions of the molecular beam, laser beam, and surface are shown. (b) The speed distributions at two surface temperatures (T_s) obtained by taking a narrow, 20 pixel wide, slice in the x-direction through the center of the feature (at y = 680 pixels). The blue lines show Maxwell-Boltzmann fits to the experimental data, and the temperature of the gas (T_g) obtained from the fit is also shown.

in the x- and y-directions, respectively, centered at x = 300 and y = 680. We then determined the ion signal in this integration region for each individual ion image as we varied the delay between the molecular beam dosing pulse and the ionization laser pulse.

Figure 5 shows kinetic traces obtained in this way for surface temperatures from 613 K to 713 K for CO desorption from Pd(111). We extract the 1st order rate constants at each surface temperature by fitting the experimental time dependent signal with a function formed by the convolution of our measured incident beam shape with a single exponential decay, in a similar manner to that used by Golibrzuch *et al.*[4] The molecular beam pulse shape used in the convolution is seen in Figure 5(f)—at this surface temperature (973 K), the residence time on the surface is much shorter than the pulse duration of the molecular beam. We used multiple Gaussian functions

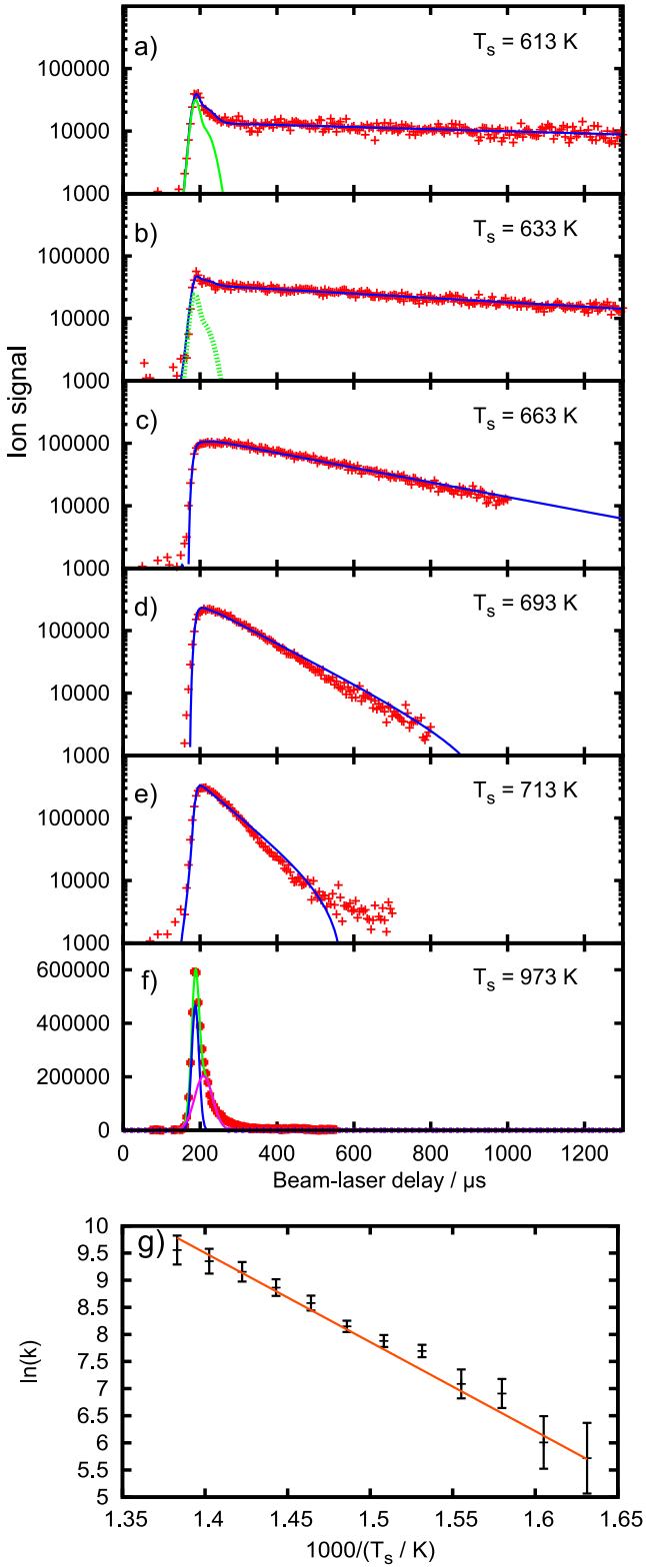

FIG. 5. Kinetics traces for CO desorbing from Pd(111). (a)-(e) Traces at different T_s, where the residence time varies from hundreds to tens of microseconds. Experimental data are shown with red points. Fits of the model to the data are shown in blue. At 613 K and 633 K, a significant component of the signal at early times is due to directly scattered molecules; this contribution to the signal is shown by the green lines. (f) The molecular beam shape is determined by measuring the desorption kinetics at high surface temperature (973 K), where the lifetime of CO on the surface is very short, and modeled using three Gaussian functions. (g) The Arrhenius plot of the surface temperature dependent CO desorption rate constants. The asymptotic standard errors shown are determined from the kinetic fits.

to fit this form and used the fitted function to carry out the convolution analytically.

The 1st order rate coefficients obtained in this way can be plotted in an Arrhenius form—Fig. 5(g). The activation energy and the pre-factor determined from the fit are $E_a = 1.29 \pm 0.03$ eV and $A = (2 \pm 1) \times 10^{13}$ s^{-1}, respectively. We used the same procedure to determine the desorption pre-exponential factor and the activation energy of CO desorption from Pt(111): $E_a = 1.28 \pm 0.02$ eV and $A = (5.9^{+5.4}_{-2.8}) \times 10^{13}$ s^{-1}.

Measurement of the desorption kinetics of adsorbed molecules provides information about the Arrhenius pre-exponential factor and the activation energy for the desorption process. Since there is no barrier to adsorption, the activation energy is closely related to the binding energy of the molecule to the surface. This allows us to compare to different kinds of previous studies, as both the desorption kinetics and the binding energy of CO on Pd(111) and Pt(111) have been investigated previously in detail.

The results found in this experiment for CO desorption from Pt(111) are in excellent agreement with the most readily comparable work of Ref. 4 ($E_a = 1.27 \pm 0.07$ eV, $A = 3.5^{+7.2}_{-2.7} \times 10^{13}$ s^{-1}). In that paper, Golibrzuch *et al.* also summarized the available literature for CO/Pt(111).[4] We attribute the observation of single exponential kinetics in the current experiment to the difference in quality of the surfaces used for the two experiments. The surface used here is much flatter than that used in the earlier experiments, with a much lower step density. The lower step density means that we are unable to observe the step-to-terrace hopping dynamics and observe only desorption from the terrace sites. Our results for CO desorption from Pd(111) are also in good agreement with some of the previously published results. For example, we can use transition state theory[4,45] to derive the CO binding energy to Pd(111) and compare to other studies. Using a 2D gas partition function for adsorbed CO, we obtain a binding energy of 1.566 ± 0.003 eV, in good agreement with the recent calorimetric data ((1.55 ± 0.04) eV).[28,29] (We note that one might also choose other forms of the partition function, but we found that for the case of CO desorption from Pt(111), this introduced only a small systematic error (0.04 eV) in the determination of the binding energy.[4]) For Pd(111), Ertl and co-workers reported an (isosteric) energy of adsorption of (34 ± 1) kcal/mol (1.47 eV), determined via measurements of adsorption isotherms.[23,24] Guo and Yates used TPD to determine a zero coverage desorption activation energy of 35.5 kcal/mol (1.54 eV) and a frequency factor $A = 10^{13.5}$ s^{-1}, the pre-factor was reported to vary strongly with coverage.[25] Goodman and co-workers, also using TPD, determined an isosteric heat of adsorption of 30 kcal/mol (1.30 eV).[26,27]

The good agreement between previous work and the desorption activation energies and pre-exponential factors measured using our ion-imaging based method supports the conclusion that this new technique is accurate.

APPLICATION: VELOCITY MAP IMAGING OF WATER SCATTERING

Velocity map imaging (VMI) has largely become the method of choice when performing chemical dynamics experiments with ion imaging. In the VMI mode, the velocity resolution is improved compared to the spatial imaging mode used in the previous section to study CO trapping-desorption by projecting all ions with a given velocity onto the same point on the detector, independent of their initial position in the extraction region. This removes the spread at the detector due to the spatial extent of the sample being probed. VMI thus offers potential improvements in speed and angular resolution that could make it easier to observe dynamical fingerprints appearing in the scattering process.

The instrument presented in this work can also be operated in the VMI mode. This is achieved by switching on an Einzel lens located between the extractor grid and the imaging detector. Due to the unknown magnification factor of the Einzel lens, VMI requires calibration of the velocity space. This can be carried out either using a known system (e.g., well characterized photodissociation) or by switching between ion imaging and VMI for the same system. The switch is straightforward when using homogeneous extraction fields with an Einzel lens, as only the voltage on the Einzel lens need be changed. In order to avoid lens aberrations but have a wide acceptance angle we use a cylindrical lens geometry for the Einzel lens as opposed to the thin plate electrodes more commonly used in gas-phase VMI. When operating in the VMI mode we reduce our acceptance angle to about 90°, from 120° allowed when operating in the ion imaging mode, to avoid the edge effects of the lens.

We demonstrate the VMI capabilities of the machine with measurements on the inelastic scattering of water from Pt(111). Here, a molecular beam of water was produced by passing helium through a reservoir of liquid water in a miniature bubbler, resulting in a beam of 0.4% H_2O in He. fs-MPI was effective in ionizing water—note REMPI of water is difficult. The Pt(111) surface was prepared in a similar manner to that described in the previous section.

In Fig. 6, we compare data obtained in spatial imaging and VMI modes for H_2O scattering from Pt(111), again using the side beam, which allows us to more easily identify directly scattered H_2O molecules at the specular angle. Figure 6(a) shows images obtained in the spatial imaging mode for H_2O/Pt(111) where the incident beam and inelastically scattered molecules are clearly seen. The incident beam is labeled I, the scattered molecules S, and the background thermal H_2O "BU" in Figure 6(a). The same features can also be seen in the VMI mode (Figure 6(b)). Note how their positions in the image have changed due to the shift from real space to velocity space. In both spatial and VMI, the laser focus was translated across the detection region during the measurement and the images summed over the laser focus position. The magnification factor of the VMI is rather small in the current setup, due to the short length of the flight tube; consequently, the spots in the image are small. In both images, the peak of the directly scattering molecules' scattered distribution lies, as expected, near to the specular angle.

We extracted speed distributions from the VMI image, shown in Figure 6(c), by performing radial integrations over 20° sectors centered on the incident beam, the scattering

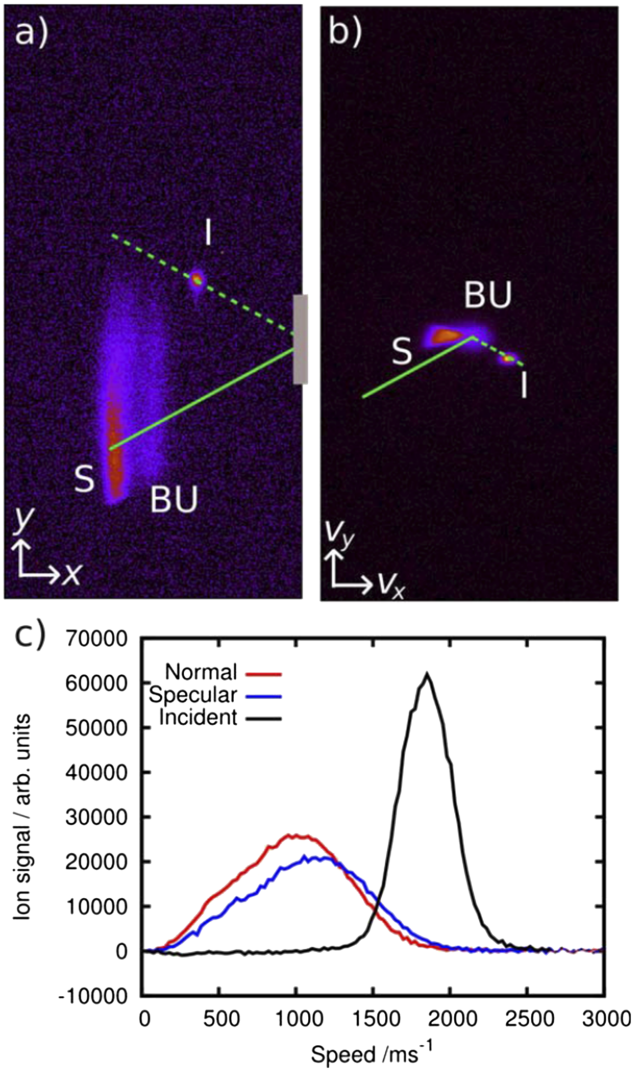

FIG. 6. (a) Spatial and (b) velocity mapped images for H_2O scattered from Pt(111) (T_s = 373 K). The incident beam (I), scattered molecules (S), and background build up (BU) are labeled. (c) shows speed distributions from the VMI image for 20° sectors centered on the incident beam, the specular scattering angle, and the normal to the surface.

signal at the surface normal, and at the specular angle. The mean translational speeds (energies) determined by numerical integration of the slices are as follows: for the incident molecular beam: 1850 ms^{-1} (0.33 eV), for the specularly scattered H_2O: 1080 ms^{-1} (0.11 eV), and for H_2O scattered near to the surface normal: 980 ms^{-1} (0.09 eV). The lower final translational energy, E_f, for molecules scattered closer to the surface normal is consistent with the observations of Hurst *et al.* for direct scattering of Ar from Pt(111).[46] The mean energy loss of the scattered molecules during the collision appears high compared to the Baule limit,[47] which predicts a final translational energy $E_f = 0.24$ eV for scattering of H_2O from Pt. The spread in the final translational energy is also large when compared to that observed in rotationally resolved scattering of diatomic molecules.[14,48] We attribute this larger spread to the use of fs-MPI, where all final rotational states of the scattered H_2O molecules are detected. As each rotational state will have a different velocity distribution, the total velocity distribution is broader than that of any single state. The total energy loss is, as expected, also greater than that for rotationally elastic scattering, where final translational energies close to the Baule limit are often observed.[14,48]

SUMMARY

We have reported the details of a new instrument which uses ion imaging techniques to study the molecular beam surface scattering and surface reaction kinetics. While not the first report of imaging detection for surface scattering experiments, the approach presented here has several advantages. For example, the chosen geometry, combined with slicing, means that with every laser shot one obtains an image that can be used to determine the speed of the detected ions. This is the key information needed to convert density to flux and detection-time to residence-time, the experimental quantities needed for accurate kinetics. This implementation of ion imaging also provides dramatically reduced measurement times compared to experiments using rotatable detectors with electron ionization or two-laser tagging experiments. Another advantage is the use of fs-MPI, which allows velocity-selective residence time measurements to be extended to almost any chemical species. The time resolution of the kinetics experiments shown in this paper is also higher than in the previous work, currently limited to ca. 20 μs by the width of the molecular beam pulse. This means reactions can be measured over a wider range of surface temperatures. This is important as surface conditions, and thereby reaction mechanisms, can vary with the surface temperature. Further improvements in the temporal resolution are possible using a slotted chopper wheel to both shorten the dosing pulse and improve its shape. The method is also compatible with VMI, which offers a higher velocity resolution, improved signal-to-noise as the ions are detected over a small region of the detector, and the ability to measure velocity distributions without knowing the precise position of the crystal surface or the laser beam as the velocities are defined relative to the image center. In the current setup, the magnification factor is too small, and further developments will include a longer flight tube to increase the magnification factor.

ACKNOWLEDGMENTS

We acknowledge the financial support of the Deutsche Forschungsgemeinschaft (DFG), Niedersächsisches Ministerium für Wissenschaft und Kultur, and the Alexander-von-Humboldt-Stiftung.

[1] O. Bünermann, H. Jiang, Y. Dorenkamp, A. Kandratsenka, S. M. Janke, D. J. Auerbach, and A. M. Wodtke, Science **350**, 1346–1349 (2015).
[2] C. T. Rettner, F. Fabre, J. Kimman, and D. J. Auerbach, Phys. Rev. Lett. **55**(18), 1904–1907 (1985).
[3] J. Werdecker, P. R. Shirhatti, K. Golibrzuch, C. Bartels, A. M. Wodtke, and D. J. Harding, J. Phys. Chem. C **119**(26), 14722–14727 (2015).
[4] K. Golibrzuch, P. R. Shirhatti, J. Geweke, J. Werdecker, A. Kandratsenka, D. J. Auerbach, A. M. Wodtke, and C. Bartels, J. Am. Chem. Soc. **137**(4), 1465–1475 (2015).
[5] R. Bisson, M. Sacchi, and R. D. Beck, Phys. Rev. B **82**, 121404(R) (2010).
[6] P. R. Shirhatti, J. Geweke, C. Steinsiek, C. Bartels, I. Rahinov, D. J. Auerbach, and A. M. Wodtke, J. Phys. Chem. Lett. **7**(7), 1346–1350 (2016).

[7]C. T. Rettner, H. A. Michelsen, and D. J. Auerbach, J. Chem. Phys. **102**(11), 4625–4641 (1995).
[8]J. E. Hurst, L. Wharton, K. C. Janda, and D. J. Auerbach, J. Chem. Phys. **83**(3), 1376–1381 (1985).
[9]K. Golibrzuch, A. Kandratsenka, I. Rahinov, R. Cooper, D. J. Auerbach, A. M. Wodtke, and C. Bartels, J. Phys. Chem. A **117**(32), 7091–7101 (2013).
[10]P. R. Shirhatti, J. Werdecker, K. Golibrzuch, A. M. Wodtke, and C. Bartels, J. Chem. Phys. **141**(12), 124704 (2014).
[11]L. K. Verheij, J. Lux, A. B. Anton, B. Poelsma, and G. Comsa, Surf. Sci. **182**, 390–410 (1987).
[12]M. P. D'Evelyn and R. J. Madix, Surf. Sci. Rep. **3**, 413–495 (1984).
[13]F. Zaera, Surf. Sci. Rep. **72**(2), 59–104 (2017).
[14]D. J. Harding, J. Neugebohren, D. J. Auerbach, T. N. Kitsopoulos, and A. M. Wodtke, J. Phys. Chem. A **119**(50), 12255–12262 (2015).
[15]G. Ertl, M. Neumann, and K. M. Streit, Surf. Sci. **64**, 393–410 (1977).
[16]H. Hopster and H. Ibach, Surf. Sci. **77**, 109–117 (1978).
[17]P. R. Norton, J. W. Goodale, and E. B. Selkirk, Surf. Sci. **83**, 189–227 (1979).
[18]T. H. Lin and G. A. Somorjai, Surf. Sci. **107**, 573–585 (1981).
[19]D. H. Winicur, J. Hurst, C. A. Becker, and L. Wharton, Surf. Sci. **109**, 263–275 (1981).
[20]B. E. Hayden and A. M. Bradshaw, Surf. Sci. **125**, 787–802 (1983).
[21]C. T. Campbell, G. Ertl, H. Kuipers, and J. Segner, Surf. Sci. **107**, 207–219 (1981).
[22]J. Harris and A. C. Luntz, J. Chem. Phys. **91**(10), 6421–6428 (1989).
[23]G. Ertl and J. Koch, Z. Naturforsch. **25**, 1906–1911 (1970).
[24]H. Conrad, G. Ertl, J. Koch, and E. E. Latta, Surf. Sci. **43**, 462–480 (1974).
[25]X. Guo and J. T. Yates, Jr., J. Chem. Phys. **90**(11), 6761–6766 (1989).
[26]W. K. Kuhn, J. Szanyi, and D. W. Goodman, Surf. Sci. **274**, L611–L618 (1992).
[27]J. Szanyi, W. K. Kuhn, and D. W. Goodman, J. Vac. Sci. Technol., A **11**(4), 1969–1974 (1993).
[28]J. H. Fischer-Wolfarth, J. Hartmann, J. A. Farmer, J. M. Flores-Camacho, C. T. Campbell, S. Schauermann, and H. J. Freund, Rev. Sci. Instrum. **82**(2), 024102 (2011).
[29]J. M. Flores-Camacho, J. H. Fischer-Wolfarth, M. Peter, C. T. Campbell, S. Schauermann, and H. J. Freund, Phys. Chem. Chem. Phys. **13**(37), 16800–16810 (2011).
[30]T. E. Madey, J. J. Czyzewski, and J. T. Yates, Surf. Sci. **49**, 465–496 (1975).
[31]M. Menges, B. Baumeister, K. Al-Shamery, H.-J. Freund, C. Fischer, and P. Andresen, Surf. Sci. **316**, 103–111 (1994).
[32]M. Wilde, K. Fukutani, Y. Maruta, M. Kampling, K. Al-Shamery, and H.-J. Freund, Surf. Sci. **427-428**, 27–33 (1999).
[33]A. R. Burns, Surf. Sci. **280**, 349–358 (1993).
[34]D. W. Chandler and P. L. Houston, J. Chem. Phys. **87**(2), 1445–1447 (1987).
[35]A. T. J. B. Eppink and D. H. Parker, Rev. Sci. Instrum. **68**(9), 3477–3484 (1997).
[36]S. Kauczok, N. Godecke, A. I. Chichinin, M. Veckenstedt, C. Maul, and K. H. Gericke, Rev. Sci. Instrum. **80**(8), 083301 (2009).
[37]M. D. Kershis, D. P. Wilson, M. G. White, J. J. John, A. Nomerotski, M. Brouard, J. W. Lee, C. Vallance, and R. Turchetta, J. Chem. Phys. **139**(8), 084202 (2013).
[38]S. P. K. Koehler, Y. Ji, D. J. Auerbach, and A. M. Wodtke, Phys. Chem. Chem. Phys. **11**(35), 7540 (2009).
[39]Y. Ji, S. P. K. Koehler, D. J. Auerbach, and A. M. Wodtke, J. Vac. Sci. Technol., A **28**(4), 807–813 (2010).
[40]S. Abujarada, H. Al Salem, U. K. Chohan, G. L. Draper, and S. P. Koehler, J. Chem. Phys. **145**(18), 184201 (2016).
[41]C. H. Hoffman and D. J. Nesbitt, J. Phys. Chem. C **120**(30), 16687–16698 (2016).
[42]D. Corr and D. C. Jacobs, Rev. Sci. Instrum. **63**(3), 1969–1972 (1992).
[43]K. Tonokura and T. Suzuki, Chem. Phys. Lett. **224**, 1–6 (1994).
[44]C. R. Gebhardt, T. P. Rakitzis, P. C. Samartzis, V. Ladopoulos, and T. N. Kitsopoulos, Rev. Sci. Instrum. **72**(10), 3848–3853 (2001).
[45]J. C. Tully, Surf. Sci. **299-300**, 667–677 (1994).
[46]J. E. Hurst, L. Wharton, K. C. Janda, and D. J. Auerbach, J. Chem. Phys. **78**(3), 1559–1581 (1983).
[47]B. Baule, Ann. Phys. **349**, 145–176 (1914).
[48]K. Golibrzuch, P. R. Shirhatti, I. Rahinov, D. J. Auerbach, A. M. Wodtke, and C. Bartels, Phys. Chem. Chem. Phys. **16**(16), 7602–7610 (2014).